

Magnon heat transport in a 2D Mott insulator

Wen O. Wang,^{1,*} Jixun K. Ding,¹ Brian Moritz,² Edwin W. Huang,³ and Thomas P. Devereaux^{2,4,†}

¹*Department of Applied Physics, Stanford University, Stanford, CA 94305, USA*

²*Stanford Institute for Materials and Energy Sciences,*

SLAC National Accelerator Laboratory, 2575 Sand Hill Road, Menlo Park, CA 94025, USA

³*Department of Physics and Institute of Condensed Matter Theory,
University of Illinois at Urbana-Champaign, Urbana, IL 61801, USA*

⁴*Department of Materials Science and Engineering, Stanford University, Stanford, CA 94305, USA*

(Dated: November 3, 2021)

Whether or not anomalies in the thermal conductivity from insulating cuprates can be attributed to antiferromagnetic order and magnons in a 2D Mott insulator remains an intriguing open question. To shed light on this issue, we investigate the thermal conductivity κ and specific heat c_v of the half-filled 2D single-band Hubbard model using the numerically exact determinant quantum Monte Carlo algorithm and maximum entropy analytic continuation. Both c_v and κ possess two peaks as a function of temperature, with scales related to the Hubbard interaction energy U and spin superexchange energy J , respectively. At low temperatures where the charge degrees of freedom are gapped-out, our results for the contribution to both c_v and the Drude weight associated with κ from the kinetic energy agree well with spin-wave theory for the spin- $\frac{1}{2}$ antiferromagnetic Heisenberg model.

I. INTRODUCTION

The effects of magnetic ordering on transport in the high- T_c cuprates is a topic of great interest. For undoped strongly correlated systems that are insulating due to Mott physics, heat transport can be measured to probe the excitations [1–5], in analogy to how charge transport probes excitations in the metallic phase. For a wide range of insulating antiferromagnetic cuprates, a general two-peak structure appears in the temperature dependence of thermal conductivity. A low-temperature phonon-related peak at $\sim 25K$ is present in both in-plane and out-plane thermal conductivity and an additional anomalously broad peak at temperature $\sim 250K$ has been observed in the in-plane thermal conductivity [3, 4, 6–8]. While considerable experimental evidence suggests that this high temperature anomaly arises from magnons or magnetic excitations [3, 6, 8, 9], its origin remains unclear [10, 11]. Resolving this debate about the origin of the anomalous peak and understanding its microscopic dynamics requires further study.

The calculation of transport properties in strongly correlated many-body systems presents a formidable challenge. For an antiferromagnetic Mott insulator the typical theoretical description of thermal transport begins by applying spin-wave theory to an antiferromagnetic Heisenberg model, which leads to low-energy dispersive magnetic excitation – magnons. Boltzmann theory can be applied, assuming weakly interacting and well-defined magnons [8, 12–14]; however, heat transport remains difficult to calculate, since we lack precise information about magnon scattering. Attempts to study thermal transport of magnons often involve taking various limits [15–17].

There also are theories for magnon thermal transport in quasi-1D systems [18–20]. Nevertheless, a numerically exact study of heat transport of a 2D Mott insulator, based on the many-body Kubo formula for thermal conductivity, has been lacking and we attempt to address this here.

The Hubbard model has been widely studied as a simplified description of the electronic properties of high- T_c cuprates [21, 22]. Although the model lacks an analytic solution in 2D, several unconventional transport phenomena in cuprates are successfully captured in numerical simulations [23–25] and in cold atom experiments [26–28]. In a previous work by some of us [23], Determinant quantum Monte Carlo algorithm [29, 30] (DQMC) and maximum entropy analytic continuation (MaxEnt) [31, 32] are utilized to investigate the optical conductivity, successfully finding strange metallicity in the doped model and insulating behavior at half-filling.

DQMC is a numerically exact algorithm and is especially efficient for calculation of the half-filled Hubbard model. We study a model with particle-hole symmetry (only nearest-neighbor hopping) such that the model is sign-problem free [33]. In the strong correlation limit $t/U \ll 1$ and low energy limit $T/U \ll 1$, by projecting out the doubly-occupied states, the effective model is the spin- $\frac{1}{2}$ antiferromagnetic Heisenberg model [34], with spin exchange energy $J = 4t^2/U$. Here t is the nearest-neighbor hopping energy, U is the Coulomb interaction and T is the temperature. In the Hubbard model with strong couplings, the non-zero-temperature maximum of the local moment $\langle m_z^2 \rangle$ [35] and a sharp peak of the spin-spin correlator $S(\mathbf{q})$ at $\mathbf{q} = (\pi, \pi)$ in DQMC [35–38] convincingly demonstrate the formation of antiferromagnetic magnons at temperature scales below J . With MaxEnt [31, 32], the dynamical spin structure factor $S(\mathbf{q}, \omega)$ has been calculated [39–41] for the undoped Hubbard model, where the results agree with

* wenwang.physics@gmail.com

† tpd@stanford.edu

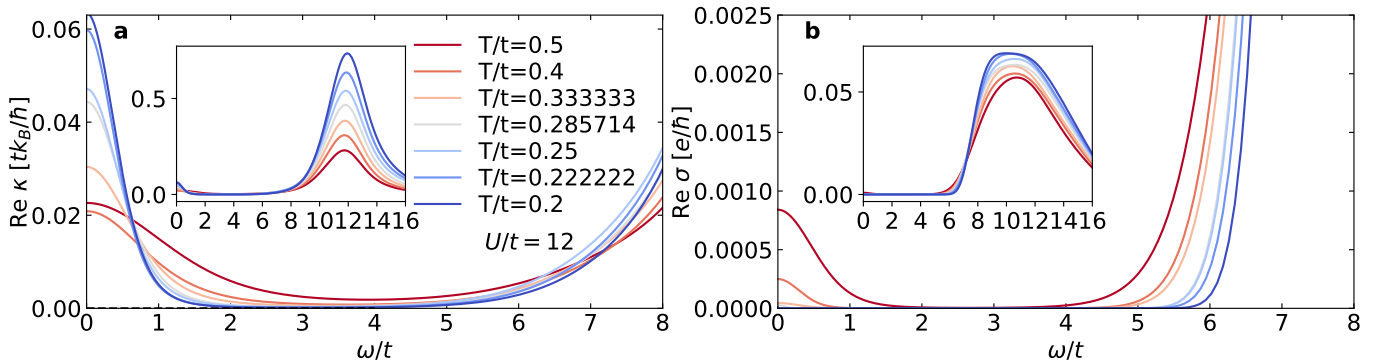


FIG. 1. Frequency dependence of the thermal conductivity $\kappa(\omega)$ (a) and optical conductivity $\sigma(\omega)$ (b) [23] for the half-filled Hubbard model with $U/t = 12$ at different temperatures. Simulation cluster of size 8×8 . The insets for (a) and (b) are profiles over a wider energy range to show the high frequency behavior.

spin-wave theory.

DQMC is well suited to study transport properties at half-filling due to lack of a sign problem at half-filling, enabling simulation on large lattices and low temperatures. With analytic continuation of unequal-time measurements, possible via the MaxEnt [31, 32] method, dynamical response functions such as the thermal conductivity may be computed. We are thus motivated to use DQMC and MaxEnt to investigate thermal transport properties of the half filled Hubbard model, particularly when antiferromagnetic correlations are strong [15, 42, 43]. Calculating thermal conductivity requires measuring heat current-heat current correlation functions, which involve observables with up to eight fermion operators. In the Supplementary Material [44], we discuss the methodology and challenges of the calculation, including an analysis of Trotter and finite-size errors.

In this paper, we observe a Drude peak in the thermal conductivity $\kappa(\omega)$ at $\omega = 0$ in undoped single-band 2D Hubbard model at temperatures below the spin exchange energy J . For the temperature dependence of the DC limit κ , we find a two-peak structure that is also observed in the temperature dependence of the specific heat c_v . The interaction and temperature dependence of these peaks are analyzed by comparing the results to purely interacting model at high temperatures and to the Heisenberg model at low temperatures. At low temperatures, we find our results of the kinetic parts of both c_v and the Drude weight of κ agree with predictions of spin-wave theory. We conclude with a discussion of possible limitations of our methods and possible future efforts on this topic.

II. RESULTS

Figure 1 shows the temperature evolution of the frequency dependence of the thermal conductivity $\kappa(\omega)$ (a) and optical conductivity $\sigma(\omega)$ [23]. The Hubbard peak at $\omega \sim U$ appears in both $\kappa(\omega)$ and $\sigma(\omega)$, where U is the interaction strength in Hubbard model. As temperature T

decreases, low-frequency $\sigma(\omega)$ shows insulating behavior, while $\kappa(\omega)$ shows a Drude peak close to $\omega = 0$, indicating that the antiferromagnetic magnons carry heat but no charge. The low-frequency Drude peak of $\kappa(\omega)$ becomes sharper as temperature decreases, reflecting well-defined magnons with a scattering rate decreasing as $T \rightarrow 0$.

We now turn to the results of specific heat c_v and the DC limit of $\kappa(\omega = 0)$, results of which are shown in Fig. 2(a) and (c). For convenience we use κ for the DC limit $\kappa(\omega = 0)$ throughout the paper. To understand the temperature dependence, we separate out the kinetic (K) and potential contributions (P) to c_v and κ [47, 48] in Fig. 2(b) and (d), by splitting the total energy H and defining the hopping energy as the kinetic energy H_K and the electron-electron interaction as the potential energy H_P . The kinetic part and potential part of c_v , named as c_K and c_P , are defined as the derivative of the corresponding energy with respect to temperature.

In order to separate the kinetic part and potential part in κ we need to define the kinetic energy current operator \mathbf{J}_K and potential energy current operator \mathbf{J}_P . However, we can not use the equation of continuity $\partial H_{K/P}/\partial t = -\nabla \cdot \mathbf{J}_{K/P}$ to define them since $H_{K/P}$ are not themselves conserved quantities. However, the total energy current operator is conserved and well-defined using the equation of continuity, and can be readily separated into two parts. We defined the two-fermion term $\propto t^2$ as the kinetic energy current \mathbf{J}_K and the four-fermion term $\propto Ut$ as the potential energy current \mathbf{J}_P , in analogy to how the Hamiltonian is split into H_K and H_P . Therefore we can define the longitudinal kinetic/potential-energy conductivities $\kappa_{K/P} = -\langle J_{K/P,x} \rangle / \partial_x T$ along the x direction. Details of these definitions are provided in the Supplementary Material [44].

For each U in Fig. 2(a), we can observe two peaks appear at two different temperatures for c_v , consistent with previous studies [35, 49]: A low-temperature peak associated with the spin exchange energy $J = 4t^2/U$, reflecting the formation of antiferromagnetic magnons as T decreases; A high-temperature peak associated with the Coulomb interaction U , reflecting the suppression of

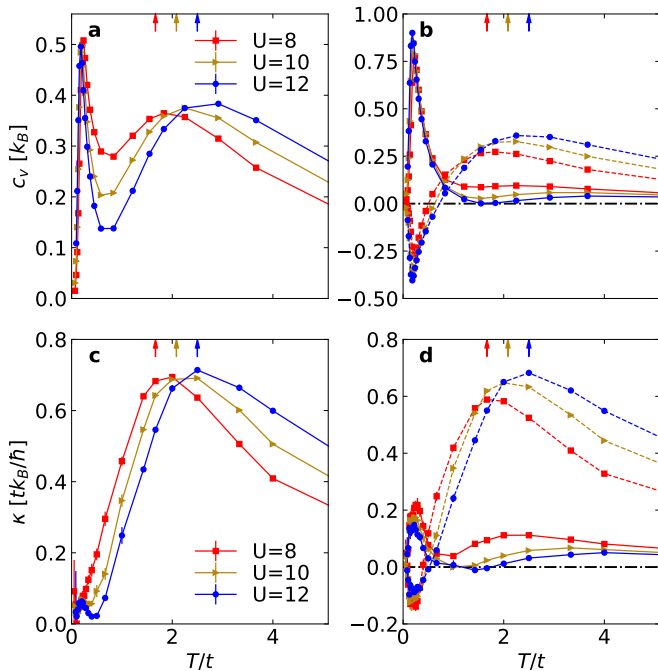


FIG. 2. Specific heat c_v and DC thermal conductivity κ for the half-filled Hubbard model with $U/t = 8, 10, 12$. (a) The total specific heat c_v calculated from finite difference, in which we choose two adjacent temperatures T_1 and T_2 and measure the energy difference, $c_v((T_1 + T_2)/2) = \delta E/\delta T = (\langle H \rangle(T_1) - \langle H \rangle(T_2))/(T_1 - T_2)$. (b) The kinetic part c_K (solid lines) and potential part c_P (dashed lines) of the specific heat c_v calculated by finite difference. (c) The total DC thermal conductivity κ . (d) The kinetic part κ_K (solid lines) and potential part κ_P (dashed lines) of κ calculated from the MaxEnt analytic continuation of the imaginary time correlators. Arrows point at $T = U/4.8$, corresponding to peak positions of the specific heat for the $t = 0$ single-site Hubbard model. The same color (marker) represents the same U . For c_v , c_K and c_P calculated from finite difference, the error has been calculated by propagating the standard error from jack-knife resampling [45], but smaller than the size of the data points. The error bars for the results for κ , κ_K and κ_P represent ± 1 bootstrap standard error [23]. Simulation cluster size is 8×8 .

double occupancy as T decreases. The high-temperature peak positions T_{high} are close to $U/4.8$ [35], which is the predicted peak position of the $t = 0$ purely interacting Hubbard model.

In semiclassical kinetic theory, for a dilute gas, κ is related to c_v by $\kappa = c_v \langle v \rangle l/d$ [12, 13], where $\langle v \rangle$ is the particle velocity, l is the mean free path and d is the number of dimensions. We can also see correspondence between the temperature dependence of κ and c_v : the two peaks also appear in κ at the same temperatures, shown in Fig. 2(c).

For both c_v and κ , we see that the high-temperature peak mainly comes from the potential parts c_P and κ_P respectively, as shown in Fig. 2((b)) and (d), associated with suppression of on-site double occupancy as temperature decreases. On the other hand, the low-temperature

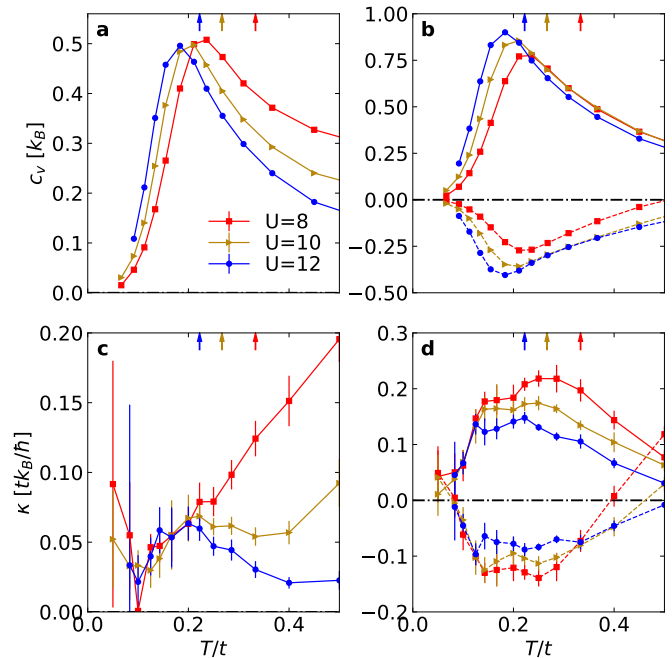


FIG. 3. Same results as Fig. 2, highlighting low temperature. Arrows point at $T = 2J/3$, the numerically predicted peak positions for the specific heat of the corresponding Heisenberg model with $J = 4t^2/U$. [46]

magnon peaks mainly come from the kinetic parts c_K and κ_K , as shown in Fig. 3((b)) and (d), since J arises from virtual hopping processes [35]. For $t/U \ll 1$ and $T \ll U$, the spin- $\frac{1}{2}$ antiferromagnetic Heisenberg model is the effective low energy model for half filled Hubbard model [34] where double occupancies are projected out. Since the potential energy involves only double occupancy terms, the magnon peaks should not come from the potential parts c_P and κ_P . However at the values of U/t considered here, double occupancy is not fully suppressed, and hence we find potential energy contributions to c_v and κ that are negative with magnitudes still significant compared with the kinetic parts, as shown in Fig. 3(b) and (d). This negative dip for c_P is also shown and discussed in [35].

We also notice that the low-temperature peak position T_{low} for both c_v and κ are almost the same, while they both deviate from the c_v peak position numerically predicted in Heisenberg model $T \sim 2J/3$ [46]. Previous works [35, 49] find closer matches between T_{low} and $2J/3$. Here, we measure c_v on a larger lattice and use a smaller imaginary time discretization $d\tau$. Therefore the difference between the previous results and our results is indeed the combined effect of the finite size effect and Trotter error, which is discussed in more details in the Supplementary Material [44]. The deviation from $2J/3$ is also understandable since the effective spin exchange energy J^* for Hubbard model with intermediate U can also deviate from the leading order approximation $J = 4t^2/U$ [40, 41]. As U increases, T_{low} approaches

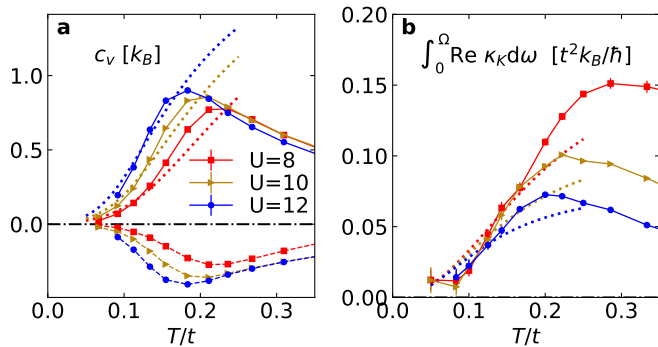


FIG. 4. Low-temperature results at half-filling compared with spin-wave theory. (a) Specific heat. Solid line: kinetic part of the specific heat c_K in Hubbard model. Dashed lines: potential part of the specific heat c_P in Hubbard model. Dotted lines: specific heat of the 2D antiferromagnetic Heisenberg model for the corresponding value of J , obtained from spin-wave theory. (b) Drude weight of the kinetic part of the thermal conductivity $\int_0^\Omega d\omega \kappa_K(\omega)$ in the Hubbard model (solid lines) compared to that obtained from spin-wave theory and the Drude formula for the 2D antiferromagnetic Heisenberg model (dotted lines). Methods in the Supplementary Material [44]. The same color (marker) represents the same U . For c_K and c_P , error bars represent ± 1 standard error determined by jackknife resampling. The error bars for the Drude weight represent 1 bootstrap standard error. Simulation cluster size for the Hubbard model is 8×8 , while the calculation for Heisenberg model is in the thermodynamic limit.

$\sim 2J/3$ as the Hubbard model is better mapped onto the Heisenberg model.

To understand the low-temperature magnon peak in c_v and κ , we compare our results with spin-wave theory for the antiferromagnetic Heisenberg model. As we previously discussed, the potential parts c_P and κ_P should not be considered as double occupancy is projected out. Therefore in Fig. 4, we compare the kinetic parts c_K and the Drude weight of κ_K with the predictions of spin-wave theory. The kinetic part of thermal Drude weight [19], defined as $\int_0^\Omega d\omega \kappa_K(\omega)$, rather than $\kappa_K(\omega)$ itself is used for comparison due to the difficulty in determining the scattering rate of the magnons in the Heisenberg model. Here, Ω is the appropriate frequency bound to include the whole low-frequency Drude peak. This scattering information is avoided in calculating $\int_0^\Omega d\omega \kappa_K(\omega)$. (See Supplementary Material [44] for details) We find that c_K and the kinetic thermal Drude weight $\int_0^\Omega d\omega \kappa_K(\omega)$ agree with the prediction from the spin-wave theory at lowest temperatures, which supports that antiferromagnetic magnons are well-formed and carry heat following Boltzmann theory and the Drude formula.

Finally, we also calculate the thermal diffusivity $D_Q = \kappa/c_v$, as shown in Fig. 5. When temperature is high enough and the system is metallic, D_Q shows a weak temperature dependence for temperatures $T/t \gtrsim 1$ similar to the charge diffusivity D [23]. This weak temperature dependence reflects the similarity of the temper-

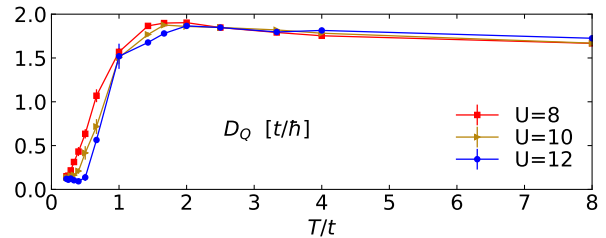


FIG. 5. Thermal diffusivity for $U/t = 8, 10, 12$. Specific heat c_v are calculated from equal-time correlations. To avoid large Trotter errors for c_v , results are shown for temperatures $T/t \geq 0.25$. Error bars represent 1 bootstrap standard error. Simulation cluster size is 8×8 .

ature dependence between κ and c_v around their high-temperature peaks. For $T/t \lesssim 1$, the Mott gap forms at the Fermi level and the system becomes insulating as indicated by the charge transport in previous work [23]. We observe that D_Q in this region drops quickly as temperature decreases, also being suppressed as the charge degrees of freedom are gapped-out.

III. DISCUSSION

In summary, we provide numerically exact results for the specific heat and analytically continued thermal conductivity for the half filled Hubbard model. We observe heat conductance by magnons in the Mott insulating antiferromagnetic phase, which appears at the same temperature as the low-temperature magnon peak of the specific heat. We find agreement of our DQMC calculations with spin-wave theory for the kinetic parts of the specific heat and the Drude weight of the thermal conductivity. Our result is also an important benchmark for other future theoretical calculation, and a reference for possible future cold atom experiments studying heat transport [50].

We here discuss the limitations of our methods. Firstly, we do not include the next nearest neighbour hopping t' in our model, which possibly takes important effects in the real materials but will lead to a sign problem in our model even at half-filling [33]. Secondly, the precision of DC limit κ at low temperatures can be affected when the true scattering rate is much lower than the temperature. Although our results of the Drude weight of κ_K from maximum entropy have a precise agreement with that obtained from the spin-wave theory of the antiferromagnetic Heisenberg model, the obtained scattering rate is difficult to verify. This is because the kernel $K(\tau, \omega)$ for converting $\chi(\tau) = \int d\omega K(\tau, \omega) \text{Re } \kappa(\omega)$, where $\chi(\tau)$ is the heat current-heat current correlator on imaginary time, limits the frequency resolution of the analytically continued data to $\sim T$. If the scattering rate decays faster than T as temperature decreases, for example $\sim T^2$ as suggested by some works [17], the Drude peak of $\kappa(\omega)$ may become much sharper than the kernel's frequency

resolution, and the frequency dependence around $\omega = 0$ will become more difficult to capture in analytic continuation of $\chi(\tau)$ at low temperatures. While the Drude weight may still be reliably calculated, the overestimation of the scattering rate may cause our results of DC limit κ to be underestimated, and future work would be needed for verification.

Other possible future directions to pursue include the investigation of the heat transport for Hubbard model with next nearest neighbour hopping t' and doping. It is an interesting question on how to understand the heat transport in a bad metal [50–52], as well as whether the usual Fermi liquid theory and Wiedemann-Franz law still hold for strongly correlated systems.

The data and analysis routines (Jupyter/Python) needed to reproduce the figures can be found at <https://doi.org/10.5281/zenodo.5305985>.

ACKNOWLEDGMENTS

We acknowledge helpful discussions with R.T.Scalettar. *Funding:* This work was supported by the U.S. Department of Energy (DOE), Office of Basic Energy Sciences, Division of Materials Sciences and Engineering. EWH was supported by the Gordon and Betty Moore Foundation EPiQS Initiative through the grants GBMF 4305 and GBMF 8691. Computational work was performed on the Sherlock cluster at Stanford University and on resources of the National Energy Research Scientific Computing Center, supported by the U.S. DOE, Office of Science, under Contract no. DE-AC02-05CH11231.

-
- [1] B. C. Sales, M. D. Lumsden, S. E. Nagler, D. Mandrus, and R. Jin, *Phys. Rev. Lett.* **88**, 095901 (2002).
- [2] R. Jin, Y. Onose, Y. Tokura, D. Mandrus, P. Dai, and B. C. Sales, *Phys. Rev. Lett.* **91**, 146601 (2003).
- [3] C. Hess, B. Büchner, U. Ammerahl, L. Colonescu, F. Heidrich-Meisner, W. Brenig, and A. Revcolevschi, *Phys. Rev. Lett.* **90**, 197002 (2003).
- [4] Y. Nakamura, S. Uchida, T. Kimura, N. Motohira, K. Kishio, K. Kitazawa, T. Arima, and Y. Tokura, *Physica C: Superconductivity* **185-189**, 1409 (1991).
- [5] S. Y. Li, L. Taillefer, C. H. Wang, and X. H. Chen, *Phys. Rev. Lett.* **95**, 156603 (2005).
- [6] K. Berggold, T. Lorenz, J. Baier, M. Kriener, D. Senff, H. Roth, A. Severing, H. Hartmann, A. Freimuth, S. Barilo, and F. Nakamura, *Phys. Rev. B* **73**, 104430 (2006).
- [7] X. F. Sun, J. Takeya, S. Komiyama, and Y. Ando, *Phys. Rev. B* **67**, 104503 (2003).
- [8] M. Hofmann, T. Lorenz, K. Berggold, M. Grüninger, A. Freimuth, G. S. Uhrig, and E. Brück, *Phys. Rev. B* **67**, 184502 (2003).
- [9] A. L. Chernyshev and W. Brenig, *Phys. Rev. B* **92**, 054409 (2015).
- [10] D. T. Morelli, J. Heremans, G. Doll, P. J. Picone, H. P. Jenssen, and M. S. Dresselhaus, *Phys. Rev. B* **39**, 804 (1989).
- [11] J. L. Cohn, C. K. Lowe-Ma, and T. A. Vanderah, *Phys. Rev. B* **52**, R13134 (1995).
- [12] C. Di Castro and R. Raimondi, “Brownian motion and transport in disordered systems,” in *Statistical Mechanics and Applications in Condensed Matter* (Cambridge University Press, 2015) p. 155–169.
- [13] N. W. Ashcroft and N. D. Mermin, “Solid state physics,” (1976).
- [14] M. Hofmann, T. Lorenz, G. S. Uhrig, H. Kierspel, O. Zabara, A. Freimuth, H. Kageyama, and Y. Ueda, *Phys. Rev. Lett.* **87**, 047202 (2001).
- [15] S. Chakravarty, B. I. Halperin, and D. R. Nelson, *Phys. Rev. B* **39**, 2344 (1989).
- [16] P. Kopietz, *Phys. Rev. B* **41**, 9228 (1990).
- [17] S. Ty and B. I. Halperin, *Phys. Rev. B* **42**, 2096 (1990).
- [18] J. V. Alvarez and C. Gros, *Phys. Rev. Lett.* **89**, 156603 (2002).
- [19] F. Heidrich-Meisner, A. Honecker, D. C. Cabra, and W. Brenig, *Phys. Rev. B* **66**, 140406 (2002).
- [20] F. Heidrich-Meisner, A. Honecker, D. C. Cabra, and W. Brenig, *Phys. Rev. Lett.* **92**, 069703 (2004).
- [21] E. Fradkin, S. A. Kivelson, and J. M. Tranquada, *Rev. Mod. Phys.* **87**, 457 (2015).
- [22] B. Keimer, S. A. Kivelson, M. R. Norman, S. Uchida, and J. Zaanen, *Nature* **518**, 179 (2015).
- [23] E. W. Huang, R. Sheppard, B. Moritz, and T. P. Devereaux, *Science* **366**, 987 (2019).
- [24] W. O. Wang, J. K. Ding, B. Moritz, E. W. Huang, and T. P. Devereaux, *npj Quantum Materials* **5**, 51 (2020).
- [25] W. O. Wang, J. K. Ding, B. Moritz, Y. Schattner, E. W. Huang, and T. P. Devereaux, *Phys. Rev. Research* **3**, 033033 (2021).
- [26] W. Xu, W. R. McGehee, W. N. Morong, and B. DeMarco, *Nature Communications* **10**, 1588 (2019).
- [27] P. T. Brown, D. Mitra, E. Guardado-Sanchez, R. Nourafkan, A. Reymbaut, C.-D. Hébert, S. Bergeron, A.-M. S. Tremblay, J. Kokalj, D. A. Huse, P. Schauf, and W. S. Bakr, *Science* **363**, 379 (2019).
- [28] M. A. Nichols, L. W. Cheuk, M. Okan, T. R. Hartke, E. Mendez, T. Senthil, E. Khatami, H. Zhang, and M. W. Zwierlein, *Science* **363**, 383 (2019).
- [29] R. Blankenbecler, D. J. Scalapino, and R. L. Sugar, *Phys. Rev. D* **24**, 2278 (1981).
- [30] S. R. White, D. J. Scalapino, R. L. Sugar, E. Y. Loh, J. E. Gubernatis, and R. T. Scalettar, *Phys. Rev. B* **40**, 506 (1989).
- [31] M. Jarrell and J. E. Gubernatis, *Physics Reports* **269**, 133 (1996).
- [32] O. Gunnarsson, M. W. Haverkort, and G. Sangiovanni, *Phys. Rev. B* **82**, 165125 (2010).
- [33] E. Y. Loh, J. E. Gubernatis, R. T. Scalettar, S. R. White, D. J. Scalapino, and R. L. Sugar, *Phys. Rev. B* **41**, 9301 (1990).
- [34] A. Auerbach, “The hubbard model and its descendants,” in *Interacting Electrons and Quantum Magnetism* (Springer New York, New York, NY, 1994) pp. 21–35.

- [35] T. Paiva, R. T. Scalettar, C. Huscroft, and A. K. McMah-
han, *Phys. Rev. B* **63**, 125116 (2001).
- [36] C. N. Varney, C.-R. Lee, Z. J. Bai, S. Chiesa, M. Jarrell,
and R. T. Scalettar, *Phys. Rev. B* **80**, 075116 (2009).
- [37] Y. F. Kung, C.-C. Chen, Y. Wang, E. W. Huang, E. A.
Nowadnick, B. Moritz, R. T. Scalettar, S. Johnston, and
T. P. Devereaux, *Phys. Rev. B* **93**, 155166 (2016).
- [38] S. R. White, D. J. Scalapino, R. L. Sugar, E. Y. Loh,
J. E. Gubernatis, and R. T. Scalettar, *Phys. Rev. B* **40**,
506 (1989).
- [39] Y. F. Kung, E. A. Nowadnick, C. J. Jia, S. Johnston,
B. Moritz, R. T. Scalettar, and T. P. Devereaux, *Phys.*
Rev. B **92**, 195108 (2015).
- [40] E. W. Huang, C. B. Mendl, S. Liu, S. Johnston, H.-C.
Jiang, B. Moritz, and T. P. Devereaux, *Science* **358**,
1161 (2017).
- [41] E. W. Huang, C. B. Mendl, H.-C. Jiang, B. Moritz, and
T. P. Devereaux, *npj Quantum Materials* **3**, 22 (2018).
- [42] H. Q. Lin and J. E. Hirsch, *Phys. Rev. B* **35**, 3359 (1987).
- [43] D. P. Arovas and A. Auerbach, *Phys. Rev. B* **38**, 316
(1988).
- [44] Supplementary Material.
- [45] J. Tukey, *Ann. Math. Statist.* **29**, 614 (1958).
- [46] J. Jaklič and P. Prelovšek, *Phys. Rev. Lett.* **77**, 892
(1996).
- [47] C. Lenihan, A. J. Kim, F. Šimkovic IV., and E. Kozik,
Phys. Rev. Lett. **126**, 105701 (2021).
- [48] R. Nourafkan and A. Tremblay, arXiv preprint
arXiv:2012.02005 (2020).
- [49] D. Duffy and A. Moreo, *Phys. Rev. B* **55**, 12918 (1997).
- [50] D. Husmann, M. Lebrat, S. Häusler, J.-P. Brantut,
L. Corman, and T. Esslinger, *Proceedings of the Na-*
tional Academy of Sciences **115**, 8563 (2018).
- [51] J. Zhang, E. D. Kountz, E. M. Levenson-Falk, D. Song,
R. L. Greene, and A. Kapitulnik, *Phys. Rev. B* **100**,
241114 (2019).
- [52] C. H. Mousatov, I. Esterlis, and S. A. Hartnoll, *Phys.*
Rev. Lett. **122**, 186601 (2019).

Supplementary Material for “Magnon heat transport in a 2D Mott insulator”

Wen O. Wang,^{1,*} Jixun K. Ding,¹ Brian Moritz,² Edwin W. Huang,³ and Thomas P. Devereaux^{2,4,†}

¹*Department of Applied Physics, Stanford University, Stanford, CA 94305, USA*

²*Stanford Institute for Materials and Energy Sciences,*

SLAC National Accelerator Laboratory, 2575 Sand Hill Road, Menlo Park, CA 94025, USA

³*Department of Physics and Institute of Condensed Matter Theory,
University of Illinois at Urbana-Champaign, Urbana, IL 61801, USA*

⁴*Department of Materials Science and Engineering, Stanford University, Stanford, CA 94305, USA*

(Dated: November 3, 2021)

I. FORMALISM

We consider specific heat in the grand canonical ensemble,

$$c_a = \frac{d}{dT} \frac{\langle H_a \rangle}{V} = -\beta^2 \frac{d}{d\beta} \frac{\langle H_a \rangle}{V} = -\beta^2 \frac{d}{d\beta} \frac{\text{tr } H_a e^{-\beta(H-\mu N)}}{V \text{tr } e^{-\beta(H-\mu N)}}, \quad (1)$$

where H is the Hamiltonian, μ is the chemical potential, N is the total number of particles in the system, and V is the volume of the system. Here, we separate the Hamiltonian into two parts, where a can be taken as K or P , representing the kinetic and potential energy terms of the Hamiltonian, or combined for the full Hamiltonian and total energy. We have

$$\frac{d}{d\beta} e^{-\beta(H-\mu N)} = (-H + N \frac{d(\beta\mu)}{d\beta}) e^{-\beta(H-\mu N)}. \quad (2)$$

So

$$\begin{aligned} & \frac{d}{d\beta} \langle H_a \rangle \\ &= \left\langle H_a (-H + N \frac{d(\beta\mu)}{d\beta}) \right\rangle - \langle H_a \rangle \left\langle -H + N \frac{d(\beta\mu)}{d\beta} \right\rangle \\ &= -(\langle H_a H \rangle - \langle H_a \rangle \langle H \rangle) + \frac{d(\beta\mu)}{d\beta} (\langle H_a N \rangle - \langle H_a \rangle \langle N \rangle). \end{aligned} \quad (3)$$

μ is tuned so that the total density remains fixed while varying the temperature. So

$$\begin{aligned} 0 &= \frac{d}{d\beta} \langle N \rangle \\ &= -(\langle NH \rangle - \langle N \rangle \langle H \rangle) + \frac{d(\beta\mu)}{d\beta} (\langle N^2 \rangle - \langle N \rangle^2). \end{aligned} \quad (4)$$

Defining $\chi_{O_1 O_2} = \beta(\langle O_1 O_2 \rangle - \langle O_1 \rangle \langle O_2 \rangle)$ in Eqs. 3 and 4, we obtain

$$c_a = \frac{\beta}{V} (\chi_{H_a H} - \frac{\chi_{H_a N} \chi_{H N}}{\chi_{N N}}). \quad (5)$$

It is obvious that the sum of the kinetic and potential terms should give back the full specific heat.

$$c = c_K + c_P. \quad (6)$$

Thus, we have two methods to calculate specific heat. One is to measure energies at different temperatures and directly calculate $\delta(E/V)/\delta T$ by choosing a reasonable finite δT . The other is through Eq. 5, which we term the fluctuation method. In theory they should be identical as $\delta T \rightarrow 0$. However, in the first method if δT is too small, c_a will be affected significantly by statistical errors in the energies. On the other hand, if the finite δT is too large, it introduces an additional source of systematic error. The second method suffers from Trotter error at low temperatures, which will introduce a divergence in c_a as $T \rightarrow 0$ [1]. (See section II)

For heat transport, we consider the response due to a temperature gradient $\nabla_\gamma T$ and electric field \mathbf{E} . We define $\bar{\mu} = \mu + e^* V$ so that $\nabla \bar{\mu} = \nabla \mu - e^* \mathbf{E}$, where e^* is the particle charge ($e^* = -e$ for electrons). We define \mathbf{J} to be the particle current operator, and also define \mathbf{J}_a , where $a = Q$ represents heat current operator, $a = K$ represents the kinetic energy current operator, and $a = P$ represents the potential energy current operator. The current responses along the α directions are defined as [2]

$$\begin{aligned} \langle J_\alpha \rangle / V &= -\beta L_{11}^{\alpha\gamma} \partial_\gamma \bar{\mu} + L_{12}^{\alpha\gamma} \partial_\gamma \beta \\ &= -\beta L_{11}^{\alpha\gamma} \partial_\gamma \bar{\mu} - L_{12}^{\alpha\gamma} \beta^2 \partial_\gamma T, \end{aligned} \quad (7)$$

$$\begin{aligned} \langle J_{a,\alpha} \rangle / V &= -\beta L_{a1}^{\alpha\gamma} \partial_\gamma \bar{\mu} + L_{a2}^{\alpha\gamma} \partial_\gamma \beta \\ &= -\beta L_{a1}^{\alpha\gamma} \partial_\gamma \bar{\mu} - L_{a2}^{\alpha\gamma} \beta^2 \partial_\gamma T. \end{aligned} \quad (8)$$

Thus, we have the longitudinal thermal and kinetic/potential-energy conductivities κ_a in zero magnetic field and zero electrical current,

$$\kappa_a = \frac{\langle J_{a,\alpha} \rangle / V}{-\partial_\alpha T} = \beta^2 (L_{a2} - \frac{L_{a1} L_{12}}{L_{11}}), \quad (9)$$

and the electric conductivity,

$$\sigma_{ele} = \frac{e^* \langle J_\alpha \rangle / V}{E_\alpha} = -\frac{e^2 \langle J_\alpha \rangle / V}{\partial_\alpha \bar{\mu}} = e^2 \beta L_{11}. \quad (10)$$

Here the coefficients L_{a1}, L_{12}, L_{11} are all longitudinal, which means $\alpha = \gamma$ in Eqs 7 and 8. The linear response

* wenwang.physics@gmail.com

† tpd@stanford.edu

coefficients can be obtained by using perturbation theory [2–4],

$$L_{11}(\omega) = \frac{1}{V\beta} \int_0^\infty dt e^{i(\omega+i0^+)t} \int_0^\beta d\tau \langle J_x(t-i\tau)J_x(0) \rangle \quad (11)$$

$$L_{a1}(\omega) = \frac{1}{V\beta} \int_0^\infty dt e^{i(\omega+i0^+)t} \int_0^\beta d\tau \langle J_{a,x}(t-i\tau)J_x(0) \rangle \quad (12)$$

$$L_{12}(\omega) = \frac{1}{V\beta} \int_0^\infty dt e^{i(\omega+i0^+)t} \int_0^\beta d\tau \langle J_x(t-i\tau)J_{Q,x}(0) \rangle \quad (13)$$

$$L_{a2}(\omega) = \frac{1}{V\beta} \int_0^\infty dt e^{i(\omega+i0^+)t} \int_0^\beta d\tau \langle J_{a,x}(t-i\tau)J_{Q,x}(0) \rangle. \quad (14)$$

These are Kubo formulas for the coefficients. We can find that in Eqs. 11-14, replacing $J_{a,x}$ by $J_{a,x} + \lambda_1 J_x$ and replacing $J_{Q,x}$ by $J_{Q,x} + \lambda_2 J_x$ for any constant λ_1 and λ_2 , leaves the results unchanged for κ_a in Eq. 9 and σ_{ele} in Eq. 10.

We consider the Hubbard model,

$$H = -t \sum_{\langle lp \rangle \sigma} \left(c_{l\sigma}^\dagger c_{p\sigma} + c_{p\sigma}^\dagger c_{l\sigma} \right) + U \sum_l \left(n_{l\uparrow} - \frac{1}{2} \right) \left(n_{l\downarrow} - \frac{1}{2} \right), \quad (15)$$

where t is the nearest-neighbour hopping and U is the on-site repulsive Coulomb interaction. $c_{l,\sigma}^\dagger$ ($c_{l,\sigma}$) is the creation (annihilation) operator for an electron at site l with spin σ , and $n_{l,\sigma} \equiv c_{l,\sigma}^\dagger c_{l,\sigma}$ is the number operator at site l . The model is placed on a square lattice and with periodic boundary conditions. Equation 15 can be separated easily into kinetic $\propto t$ and potential $\propto U$ contributions.

Therefore the local energy at site l is

$$h_l = -\frac{t}{2} \sum_{\delta,\sigma} \left(c_{l+\delta,\sigma}^\dagger c_{l,\sigma} + c_{l,\sigma}^\dagger c_{l+\delta,\sigma} \right) + U \left(n_{l\uparrow} - \frac{1}{2} \right) \left(n_{l\downarrow} - \frac{1}{2} \right), \quad (16)$$

where δ includes all position displacements for nearest neighbours. Specifically, on a 2D square lattice $\delta = +\mathbf{x}, -\mathbf{x}, +\mathbf{y}, -\mathbf{y}$, where the lattice constant is set to 1 and \mathbf{x} and \mathbf{y} are unit vectors.

We define the chemical potential as μ , the position of site l as \mathbf{r}_l and $\mathbf{R}_E = \sum_l \mathbf{r}_l h_l$. So the energy current \mathbf{J}_E

is [3]

$$\begin{aligned} \mathbf{J}_E &= i[H - \mu N, \mathbf{R}_E] = i \sum_{p,l} [h_p - \mu n_p, \mathbf{r}_l h_l] \\ &= \sum_{l,\delta_1,\delta_2 \in \{\delta\},\sigma} \left(-\frac{\delta_1 + \delta_2}{4} \right) t^2 (i c_{l+\delta_1+\delta_2,\sigma}^\dagger c_{l,\sigma} + h.c.) \\ &\quad + \frac{Ut}{4} \sum_{l,\delta \in \{\delta\},\sigma} \delta(n_{l+\delta,\sigma} + n_{l,\sigma}) (i c_{l+\delta,\sigma}^\dagger c_{l,\sigma} + h.c.) \\ &\quad - \frac{Ut}{4} \sum_{l,\delta \in \{\delta\},\sigma} \delta(i c_{l+\delta,\sigma}^\dagger c_{l,\sigma} + h.c.). \end{aligned} \quad (17)$$

Similar to the separation of H in Eq. 15, we also can separate the energy current \mathbf{J}_E into a kinetic part $\mathbf{J}_K \propto t^2$ and a potential part $\mathbf{J}_P \propto Ut$. The heat current is determined by

$$\mathbf{J}_Q = \mathbf{J}_E - \mu \mathbf{J}, \quad (18)$$

where \mathbf{J} is the particle current,

$$\begin{aligned} \mathbf{J} &= i[H - \mu N, \mathbf{R}_N] = i \sum_{p,l} [h_p - \mu n_p, \mathbf{r}_l n_l] \\ &= \frac{t}{2} \sum_{l,\delta \in \{\delta\},\sigma} \delta(i c_{l+\delta,\sigma}^\dagger c_{l,\sigma} + h.c.). \end{aligned}$$

At half-filling, $\mu = 0$. We consider the case of a bipartite cluster divided into two sublattices, A and B, where no hopping occurs between sites on the same sublattice. The particle-hole transformation can be defined as

$$d_l = \alpha_l c_{l,\sigma}^\dagger, \quad (19)$$

where $\alpha_l = 1$ for $l \in A$ and $\alpha_l = -1$ for $l \in B$. We thus have particle-hole symmetry in the grand canonical Hamiltonian $H - \mu N$ at half-filling, which means, after the transformation, the Hamiltonian remains unchanged with that appearing in Eq. 15, only with $c \rightarrow d$. It is notable that in Eq. 17, $c_{l+\delta_1+\delta_2}$ and c_l are always on the same sublattice, while $c_{l+\delta}$ and c_l are always on different sublattices. So after the particle-hole transformation, $\mathbf{J}_K \rightarrow -\mathbf{J}_K$, $\mathbf{J}_P \rightarrow -\mathbf{J}_P$, $\mathbf{J} \rightarrow \mathbf{J}$, with the operator substitution $c \rightarrow d$. So we know that particle-hole symmetry guarantees $\langle \mathbf{J}_K \mathbf{J} \rangle = \langle \mathbf{J}_P \mathbf{J} \rangle = 0$. This leads to $L_{a1} = L_{12} = 0$ in Eqs. 12 and 13. To measure κ_a and σ_{ele} , we only need to measure and apply analytic continuation for $\langle J_x(\tau)J_x \rangle$, $\langle J_{K,x}(\tau)J_{K,x} \rangle$, $\langle J_{P,x}(\tau)J_{P,x} \rangle$, and $\langle J_{E,x}(\tau)J_{E,x} \rangle$. Similarly, one can verify that $\chi_{H_a N} = 0$. So in Eq. 5, we only need to calculate the energy fluctuation function $\chi_{H_a H}$ for the specific heat.

II. TROTTER ERROR AND FINITE SIZE EFFECT

Specific heat in previous work using QMC [5, 6] indicated that the low-temperature peak position for the

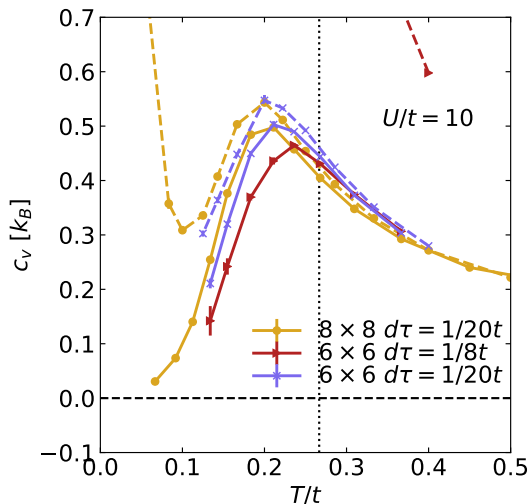


FIG. 1. Specific heat c_v calculated with three different sets of parameters including lattice sizes and $d\tau$. Solid lines: calculated from finite difference of energy. Dashed lines: calculated from energy fluctuation. Pairs of a dashed and solid lines share the same parameters. Error bars represent ± 1 standard error determined by jackknife resampling. Black dotted line indicates the temperature position $T = 2J/3$.

Hubbard model with $U/t \geq 10$ matches closely to $T_{\text{low}} \sim 2J/3$, the peak position numerically calculated in the Heisenberg model [7]. However, our result in Fig. 3 in the main text deviates from this position even for $U/t = 10$ and 12, as we simulate on a larger lattice sizes and for a smaller imaginary time discretization $d\tau$. The difference between our result and that in previous work is a combined effect of finite-size and the Trotter error, as shown in Fig. 1. The red line shows results using the same lattice size and $d\tau$ as Ref. [5]. Changes in lattice size and $d\tau$ both change the peak position to some extent; however, the qualitative behavior does not change.

Looking more closely at the Trotter error, conventional constraint for a sufficiently small $d\tau$ requires $U(d\tau)^2 \leq 1/(8t) = 1/W$, where $W = 8t$ is the non-interacting bandwidth. However, this constraint is far from sufficient for Eq. 5 (the fluctuation method), as shown in Fig. 2. For the largest value of the interaction in our study $U/t = 12$ we find that even $d\tau = 1/20t$ is not small enough to sufficiently suppress Trotter error at low temperatures $T/t < 0.2$, as shown in Fig. 2 (a). Further, the highest temperature where c_K and c_P calculated from using the fluctuation method with $d\tau = 1/20t$ start to show significant trotter error is even higher than that for c_v , as shown in in Fig. 2 (a-c). At lowest temperatures for $d\tau = 1/20t$, c_v , c_K and c_P calculated in this way diverge as $T \rightarrow 0$ [1]. However, c_v , c_K and c_P calculated from finite energy differences have far less Trotter error for the same $d\tau$.

For κ , κ_K and κ_P , the Trotter errors shown in Fig. 2 (d - f) are all of the same order as the statistic error and the difference in $d\tau$ does not affect the result qualitatively.

III. SPIN WAVE THEORY

In the limit $t/U \ll 1$, for temperature and energy much lower than U , the effective model is the spin- $\frac{1}{2}$ antiferromagnetic Heisenberg model [8]. According to spin-wave theory [9], which utilizes the Holstein-Primakoff transformation, one can obtain an approximate Hamiltonian,

$$H = E_0 + \sum_{\mathbf{k}} \hbar\omega_{\mathbf{k}} (\alpha_{\mathbf{k}}^\dagger \alpha_{\mathbf{k}} + \beta_{\mathbf{k}}^\dagger \beta_{\mathbf{k}}), \quad (20)$$

where E_0 is the ground state energy, $\alpha_{\mathbf{k}}^\dagger$ and $\beta_{\mathbf{k}}^\dagger$ create magnon excitations with wavevector \mathbf{k} and energy $\omega_{\mathbf{k}}$. The dispersion relation for both $\alpha_{\mathbf{k}}$ and $\beta_{\mathbf{k}}$ is

$$\hbar\omega_{\mathbf{k}} = JSz\sqrt{1 - \gamma_{\mathbf{k}}^2}, \quad (21)$$

where the spin exchange energy $J = 4t^2/U$, the spin $S = 1/2$, and $z = \text{dimension number} \times 2$ is the number of nearest neighbors on the lattice. $\gamma_{\mathbf{k}}$ is determined by

$$\gamma_{\mathbf{k}} = \frac{1}{z} \sum_{\delta} \cos(\mathbf{k} \cdot \delta). \quad (22)$$

In deriving this expression, our 2D square lattice has been divided into two interpenetrating sublattices. So, \mathbf{k} should be chosen in the magnetic Brillouin zone, which is formed by either sublattice with a lattice constant $\sqrt{2}$, while $\delta = +\mathbf{x}, -\mathbf{x}, +\mathbf{y}, -\mathbf{y}$ are the nearest neighbour displacements on the original lattice.

Dotted lines in Fig. 4(a) in the main text are obtained by calculating the following expression in the thermodynamic limit:

$$\begin{aligned} \frac{\partial}{\partial T} E &= \frac{1}{V} \sum_{\mathbf{k}} 2\hbar\omega_{\mathbf{k}} \frac{\partial}{\partial T} n(\mathbf{k}) = \iint d\mathbf{k} c_v(\mathbf{k}) \quad (23) \\ &= \frac{2}{4\pi^2} \int_0^{\frac{2\pi}{\sqrt{2}}} dk_{x'} \int_0^{\frac{2\pi}{\sqrt{2}}} dk_{y'} \frac{2(\hbar\omega_{\mathbf{k}})^2 / (k_B T^2) e^{\hbar\omega_{\mathbf{k}} / (k_B T)}}{(e^{\hbar\omega_{\mathbf{k}} / (k_B T)} - 1)^2}, \quad (24) \end{aligned}$$

where $n(\mathbf{k})$ is the Bose-Einstein distribution $n(\mathbf{k}) = 1/(e^{\hbar\omega_{\mathbf{k}}/k_B T} - 1)$. The factor 2 in Eq. 23 comes from the fact that there are two types of magnon excitations $\alpha_{\mathbf{k}}$ and $\beta_{\mathbf{k}}$. Here, the x' and y' directions are along the next-nearest-neighbour bonds of the original lattice, which are the nearest-neighbours of the sublattice with a distance $\sqrt{2}$.

For dotted lines in Fig. 4(b) in the main text, we use the thermal conductivity expression for the bosonic gas derived from the Boltzmann Equation [10, 11], and add the frequency dependence based on the Drude formula,

$$\kappa(\omega) = \iint d\mathbf{k} c_v(\mathbf{k}) v_{\mathbf{k},x'}^2 \frac{\tau(\mathbf{k})}{1 - i\omega\tau(\mathbf{k})} \quad (25)$$

where $v_{\mathbf{k},x'} = \frac{\hbar\partial\omega_{\mathbf{k}}}{\partial k_{x'}}$ is the magnon velocity along the x' direction, and $\tau(\mathbf{k})$ is the \mathbf{k} -dependent relaxation time.

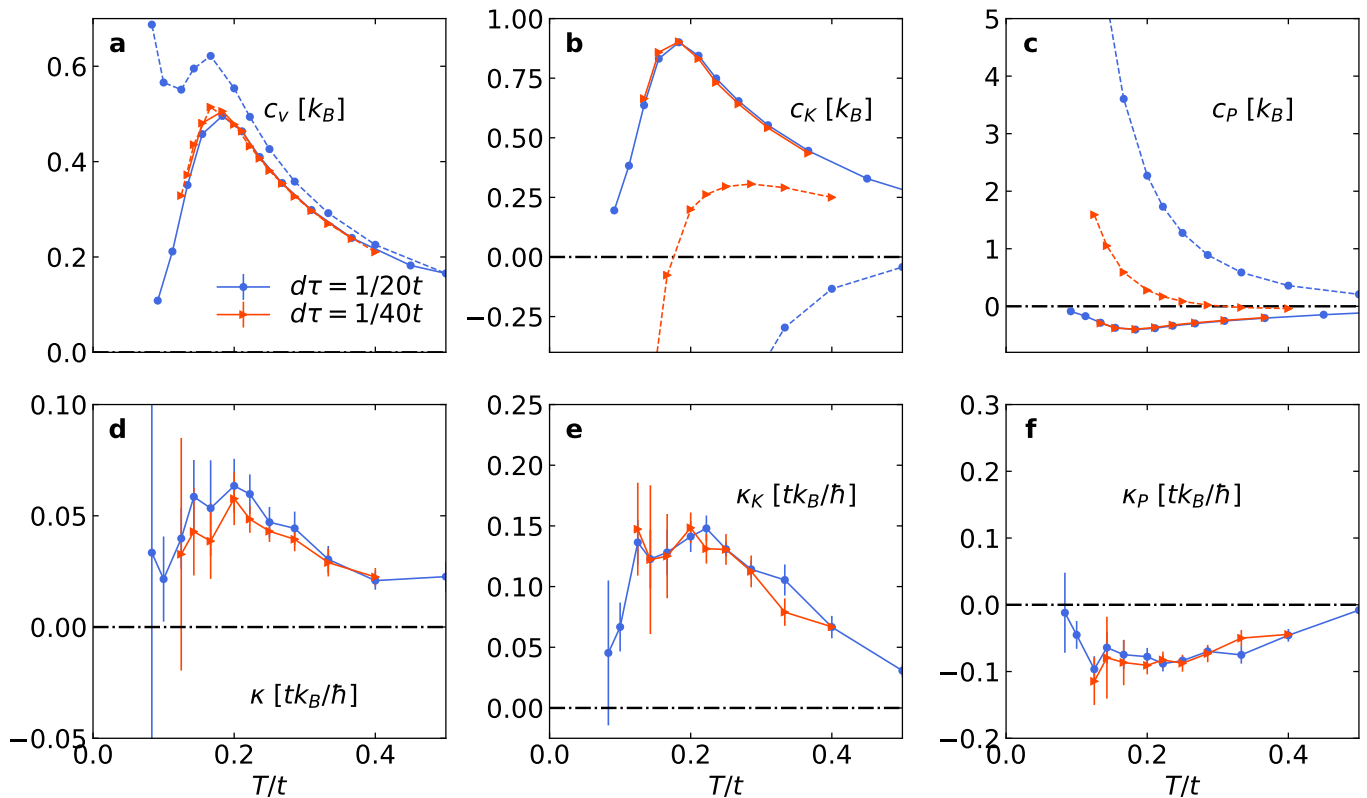


FIG. 2. Trotter error analysis. (a) c_v , (b) c_K , (c) c_P , (d) κ , (e) κ_K , and (f) κ_P calculated with $d\tau = 1/(20t)$ and $1/(40t)$. In panels a-c, solid lines are calculated from finite difference, while dashed lines are calculated from energy fluctuation in Eq. 5. Pairs of a dashed and solid lines share the same $d\tau$. For panels a-c, error bars represent ± 1 standard error determined by jackknife resampling. For panels d-f, error bars represent 1 bootstrap standard error. Interaction $U/t = 12$. Simulation cluster size is 8×8 .

As an analog, one can refer to the photonic thermal conductivity for the Debye model [12, 13]. The only unknown quantity in Eq. 25 is $\tau(\mathbf{k})$. However, we can obtain the Drude weight explicitly without knowing $\tau(\mathbf{k})$. Integrating the real part of Eq. 25 over ω gives

$$\int_0^\infty \text{Re } \kappa(\omega) d\omega = \frac{\pi}{2} \iint d\mathbf{k} c_v(\mathbf{k}) v_{\mathbf{k},x'}^2. \quad (26)$$

For the solid lines in Fig. 4(b) in the main text, we integrate the result of $\text{Re } \kappa_K(\omega)$, which is calculated from the analytic continuation of our DQMC data, to a frequency bound Ω . Ω should be high enough to include all the low-frequency Drude-like behavior, while it should also be away from high frequency behavior dominated by the higher-energy terms integrated out in deriving the Heisenberg Hamiltonian. Our choices of Ω and their relative position in the spectral of $\text{Re } \kappa_K(\omega)$ are shown in Fig. 3

IV. PARAMETERS

Measurements in the main text are evaluated with a maximum imaginary time discretization $d\tau = 0.05/t$. For high temperatures the smallest $L = \beta/d\tau$ is 20. We

measure up to 1600 Markov chains for each set of parameters at the lowest temperatures, where each Markov chain contains 2.5×10^5 unequal time measurements and $2 \times 10^5 \times L$ equal time measurements. For relatively higher temperatures, fewer Markov chains are simulated. Each Markov chain consists of 5×10^4 warm up steps and 10^6 measurement steps. Unequal time measurements are taken every 4 measurement steps.

For the model function at the highest temperature, we estimate the spectrum at infinite temperature using the momentum expansion method, as in [14]. We provide a brief summary of this method. From Eqs. 11-14, we

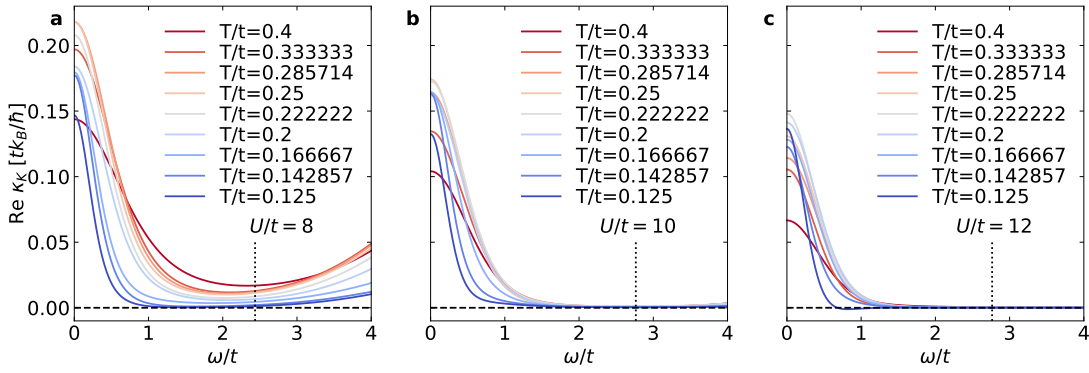


FIG. 3. Frequency dependence of $\text{Re } \kappa_K(\omega)$ at different temperatures for different U . Dotted lines indicate the position choices of the frequency bound Ω for calculation of the Drude weight.

obtain the real part of coefficient L_{aa} ,

$$\begin{aligned} & \text{Re } L_{aa}(\omega) \\ & \equiv \text{Re} \frac{1}{V\beta} \int_0^\infty dt e^{i(\omega+i0^+)t} \int_0^\beta d\tau \langle J_{a,x}(t-i\tau) J_{a,x}(0) \rangle \\ & = \frac{-\pi}{V\beta} \sum_{\xi,\eta} \frac{e^{-\beta E_\xi} (1 - e^{-\beta(E_\eta - E_\xi)})}{E_\xi - E_\eta} \|\langle \xi | J_{a,x} | \eta \rangle\|^2 \\ & \delta(\omega + E_\xi - E_\eta) \end{aligned} \quad (27)$$

$$\begin{aligned} & = \frac{1 - e^{-\beta\omega}}{\omega V\beta} \text{Re} \int_0^\infty dt e^{i(\omega+i0^+)t} \langle J_{a,x}(t) J_{a,x} \rangle \\ & = \frac{1 - e^{-\beta\omega}}{2\omega V\beta} \int_{-\infty}^\infty dt e^{i\omega t} \langle J_{a,x}(t) J_{a,x} \rangle. \end{aligned} \quad (28)$$

Here we have used

$$(e^{i(\omega+i0^+)t} \langle J_{a,x}(t) J_{a,x} \rangle)^* = e^{-i(\omega-i0^+)t} \langle J_{a,x}(-t) J_{a,x} \rangle. \quad (29)$$

At infinite high temperatures, $\beta \rightarrow 0$, Eq. 28 becomes

$$\text{Re } L_{aa}(\omega) = \frac{1}{2V} \int_{-\infty}^\infty dt e^{i\omega t} \langle J_{a,x}(t) J_{a,x} \rangle, \quad (30)$$

or

$$\langle J_{a,x}(t) J_{a,x} \rangle = \frac{V}{\pi} \int_{-\infty}^\infty d\omega e^{-i\omega t} \text{Re } L_{aa}(\omega), \quad (31)$$

which means $\langle J_{a,x}(t) J_{a,x} \rangle$ is real and even since one can prove $\text{Re } L_{aa}(\omega)$ to be even by altering ξ and η in the expression 27. Finite even order derivatives of $\langle J_{a,x}(t) J_{a,x} \rangle$

at $t = 0$ can be calculated analytically at $T = +\infty$,

$$\begin{aligned} & \frac{d^{2l}}{dt^{2l}} \langle J_{a,x}(t) J_{a,x} \rangle |_{t=0} = (-1)^l \langle (\mathcal{L}^{2l} J_{a,x}) J_{a,x} \rangle \\ & = \langle (\mathcal{L}^l J_{a,x}) (\mathcal{L}^l J_{a,x}) \rangle, \end{aligned} \quad (32)$$

which determine the Taylor expansion coefficients of $\langle J_{a,x}(t) J_{a,x} \rangle$. Here \mathcal{L} is the Liouvillian operator $\mathcal{L}O = [H, O]$ for any operator O and we have used $\langle (\mathcal{L}O_1) O_2 \rangle = -\langle O_1 (\mathcal{L}O_2) \rangle$. The highest order that we calculate is $l = 8$. We can use these coefficients to calculate the Padé approximate of $\langle J_{a,x}(t) J_{a,x} \rangle$. Within the range of t where Padé approximates converge (that is, the expansions at the two highest orders do not deviate from each other within this t range), we fit the highest order approximate to

$$\langle J_{a,x}(t) J_{a,x} \rangle = A_1 \text{sech}(\Gamma_1 t) + A_2 \text{sech}(\Gamma_2 t) \cos(\omega_2 t), \quad (33)$$

where $A_1, A_2, \Gamma_1, \Gamma_2$ and ω_2 are the fitting parameters. Therefore we have an estimate of $\langle J_{a,x}(t) J_{a,x} \rangle$ to convert to $\text{Re } L_{aa}(\omega)$ for the model function. We also notice that $\text{Re } L_{aa}(\omega)$ is positive definite in Eq. 27, so maximum entropy analytic continuation [15, 16] is applicable for $\text{Re } L_{aa}(\omega)$. We use an annealing procedure to determine the model function for other temperatures, which means we use the spectra from the current temperature as the model function for the next lower temperature. This strategy is also the same as that used in Ref. [14]. To determine the error for results from analytic continuation, we calculate 1000 bootstraps (with the same model function) and calculate the standard error from resampling.

-
- [1] R. M. Fye and R. T. Scalettar, Phys. Rev. B **36**, 3833 (1987).
 [2] B. S. Shastry, Reports on Progress in Physics **72**, 016501 (2008).
 [3] G. D. Mahan, in *Many-Particle Physics* (Springer,

- Boston, MA, 2000) pp. 109–185.
 [4] J. M. Luttinger, Phys. Rev. **135**, A1505 (1964).
 [5] T. Paiva, R. T. Scalettar, C. Huscroft, and A. K. McMahhan, Phys. Rev. B **63**, 125116 (2001).
 [6] D. Duffy and A. Moreo, Phys. Rev. B **55**, 12918 (1997).

- [7] J. Jaklič and P. Prelovšek, *Phys. Rev. Lett.* **77**, 892 (1996).
- [8] A. Auerbach, “The hubbard model and its descendants,” in *Interacting Electrons and Quantum Magnetism* (Springer New York, New York, NY, 1994) pp. 21–35.
- [9] R. Kubo, *Phys. Rev.* **87**, 568 (1952).
- [10] C. Di Castro and R. Raimondi, “Brownian motion and transport in disordered systems,” in *Statistical Mechanics and Applications in Condensed Matter* (Cambridge University Press, 2015) p. 155–169.
- [11] N. W. Ashcroft and N. D. Mermin, “Solid state physics,” (1976).
- [12] M. Hofmann, T. Lorenz, G. S. Uhrig, H. Kierspel, O. Zabara, A. Freimuth, H. Kageyama, and Y. Ueda, *Phys. Rev. Lett.* **87**, 047202 (2001).
- [13] M. Hofmann, T. Lorenz, K. Berggold, M. Grüninger, A. Freimuth, G. S. Uhrig, and E. Brück, *Phys. Rev. B* **67**, 184502 (2003).
- [14] E. W. Huang, R. Sheppard, B. Moritz, and T. P. Devereaux, *Science* **366**, 987 (2019).
- [15] M. Jarrell and J. E. Gubernatis, *Physics Reports* **269**, 133 (1996).
- [16] O. Gunnarsson, M. W. Haverkort, and G. Sangiovanni, *Phys. Rev. B* **82**, 165125 (2010).